Geologic constraints on the origin of red organic-rich material on Ceres

C. M. PIETERS [iD][1*], A. NATHUES[2], G. THANGJAM [iD][2], M. HOFFMANN[2], T. PLATZ[2],
M. C. DE SANCTIS [iD][3], E. AMMANNITO[3,4], F. TOSI[3], F. ZAMBON[3], J. H. PASCKERT[5],
H. HIESINGER[5], S. E. SCHRÖDER[6], R. JAUMANN[6], K.-D. MATZ[6], J. C. CASTILLO-ROGEZ [iD][7],
O. RUESCH[8], L. A. McFADDEN[8], D. P. O'BRIEN[9], M. SYKES[9], C. A. RAYMOND[7], and
C. T. RUSSELL[10]

[1]Brown University, DEEPS Box 1836, Providence, Rhode Island 02912, USA
[2]Max Planck Institute for Solar System Research, Goettingen, Germany
[3]Spaziali, Istituto Nazionale di Astrofisica (INAF), Rome, Italy
[4]Agenzia Spaziale Italiana (ASI), Via del politecnico s.n.c., 00133 Rome, Italy
[5]Institut für Planetologie, Westfälische Wilhelms-Universität, Münster, Germany
[6]DLR, Institute of Planetary Research, Berlin, Germany
[7]Jet Propulsion Laboratory, California Institute of Technology, Pasadena, California 91125, USA
[8]Goddard Space Flight Center, Greenbelt, Maryland 20771, USA
[9]Planetary Science Institute, Tucson, Arizona 85719, USA
[10]University of California, Los Angeles, California 90095, USA
*Corresponding author. E-mail: carle_pieters@brown.edu

(Received 17 June 2017; revision accepted 22 September 2017)

Abstract–The geologic context of red organic-rich materials (ROR) found across an elongated 200 km region on Ceres is evaluated with spectral information from the multispectral framing camera (FC) and the visible and near-infrared mapping spectrometer (VIR) of Dawn. Discrete areas of ROR materials are found to be associated with small fresh craters less than a few hundred meters in diameter. Regions with the highest concentration of discrete ROR areas exhibit a weaker diffuse background of ROR materials. The observed pattern could be consistent with a field of secondary impacts, but no appropriate primary crater has been found. Both endogenic and exogenic sources are being considered for these distinctive organic materials.

INTRODUCTION

Ceres is the largest and most massive asteroid in the solar system and is rightfully termed a dwarf planet, having undergone a complex planetary evolution based on observations of its geophysical, compositional, and geological properties. The Dawn team spent over 2 yr evaluating the character of its dark surface (Russell et al. 2016) and has documented the pervasive presence of Mg-serpentine, ammoniated clays, and opaques (De Sanctis et al. 2015; Ammannito et al. 2016) as well as notable unusual deposits of exceptionally bright carbonates within Occator crater (De Sanctis et al. 2016). Using data from Dawn's visible and near-infrared mapping spectrometer (VIR), the unmistakable absorption signature at 3.4 μm of organic materials was

also identified in the northern hemisphere of Ceres (De Sanctis et al. 2017). From the shape and character of this absorption feature, it was determined that the form of organics detected on Ceres is principally aliphatic (comprised of C-H chains).

Organics have been found or hypothesized to exist at diverse bodies across the solar system. Proposed organic features have been detected at a few asteroids with ground-based telescopes (e.g., at Themis by Rivkin and Emery [2010]; at Cybele by Licandro et al. [2011]). Organics are believed to be abundant in Kuiper belt objects (Cruikshank 1997) and their reddened spectral slope is due to an inherent property of the observed organics (e.g., Moroz et al. 1998) or possibly due to weathering (Luu and Jewitt 1996). Small amounts of organic species have been detected in Enceladus plumes

(Waite et al. 2009) and abundantly described at Titan (e.g., Soderblom et al. 2009). The regolith of comet 67P/Churyumov–Gerasimenko exhibits organic-rich species (Capaccioni et al. 2015). However, Ceres is one of the few objects at which a significant local concentration of organics has been definitively observed and mapped by spacecraft.

A spectral signature of organic materials is not detected in telescopic data of Ceres (see Rivkin et al. 2011), although ultraviolet observations obtained with the Hubble Space Telescope suggest abundant carbon, potentially in the form of graphite (Hendrix et al. 2016). However, the VIR diagnostic spectral signature at 3.4 µm is unambiguous and allowed aliphatic organics to be mapped across several specific localized areas in the northern hemisphere of Ceres. Distinctive properties of these areas near the crater Ernutet (~53°N, 45°E) were first noticed by Nathues et al. (2016) as they exhibit an unusually steep red-sloped continuum in visible wavelengths. The origin of these localized materials was explored by Nathues et al. (2016) and De Sanctis et al. (2017) and the proposed emplacement mechanisms fall into two broad categories—endogenic (formed on Ceres) or exogenic (formed elsewhere and brought to Ceres). To a first order, the former is fully consistent with Ceres' overall composition and inferred evolution characterized by Dawn as a water-rich dwarf planet that has undergone considerable internal chemical processing (Castillo-Rogez et al. Forthcoming, 2018; McSween et al. 2017). On the other hand, an exogenic origin associated with foreign debris (from low-velocity projectiles) is consistent with the localized yet dispersed pattern observed across Ceres of organics that have been superimposed on or embedded in a globally dark surface, which generally exhibits the common mineralogy found on Ceres.

In the analysis presented here, we integrate optical data from Dawn's high-altitude mapping orbit (HAMO) and low-altitude mapping orbit (LAMO) to investigate the geologic context of these organic-rich areas in greater detail. Geologic processes acting on the surface of planetary bodies like Ceres produce the varied features we see today (Williams et al. 2017). Extended impact cratering has clearly shaped and redistributed material across the airless surface for billions of years (Hiesinger et al. 2016), while internal processes have also reorganized and reprocessed subsurface materials over time (Castillo-Rogez and McCord 2010; Castillo-Rogez et al. Forthcoming, 2018). In the sections below, we evaluate the geologic context of the observed organic materials to constrain their history. The global VIR near-infrared spectroscopic data (De Sanctis et al. 2011) provide the definitive information about the presence of organic material in a spatial context, and the local

geology is further evaluated using global extended visible wavelength 7-filter framing camera (FC) color data (Sierks et al. 2011) at higher spatial resolution. Whether these organic materials were born on Ceres or elsewhere, they certainly document a prominent source of solar system organic material and thus ultimately help constrain concepts involving the origin of life.

REGIONAL CONTEXT OF CEREAN ORGANIC-RICH MATERIAL

An overview of the region on Ceres containing organic material is shown in Fig. 1. This overview provides the setting for many of the images and data discussed in subsequent sections. The area is part of the midlatitude Coniraya quadrangle (Ac-2) in the northern hemisphere of Ceres, the geology of which has been evaluated and mapped by Pasckert et al. (2017) and summarized here, while regional compositional variations are described by Raponi et al. (2017). Currently, all but one small area identified to be organic-rich (by the presence of a prominent 3.4 µm absorption band) occur in this region. The single exception is a small crater at ~10°N, 89°E on the rim of Inamahari 400 km to the southeast of Ernutet. As will be documented in the following section, all organic-rich areas identified by their diagnostic 3.4 µm absorption band also exhibit a red-sloped continuum in FC data. The specific areas identified as containing red organic-rich material (ROR) are shown in Fig. 1A and discussed in the following sections. The measured local topography (Fig. 1B) and the derived geologic units (Fig. 1C) provide the regional context for these ROR areas.

A combination of superposition relations and crater size-frequency distribution (CSFD) measurements allow the age relations to be determined among different units in the region (Pasckert et al. 2017). The overall terrain is heavily cratered with the oldest areas dating to 3.5 Ga based on CSFD measurements using the lunar-derived model (LDM; Hiesinger et al. 2016). The large complex crater Ernutet (~53 km in diameter; 53°N, 46°E) that exhibits a concentration of areas of ROR material (center of Fig. 1A) is estimated to be ~1.6 Ga (LDM) and no longer exhibits discrete ejecta deposits (Fig. 1C). The large ~50 km degraded crater to the southwest of Ernutet that also exhibits ROR is about 2.5 Ga (Nathues et al. 2016) and is thus substantially older. Although this heavily eroded crater is barely detectible in the Fig. 1A image mosaic, it is clearly discernible in topography 1B, with the portion that exhibits abundant ROR materials being slightly elevated. In contrast to these older craters, the fresh 6.5 km crater and lobate flow, located ~70 km to the
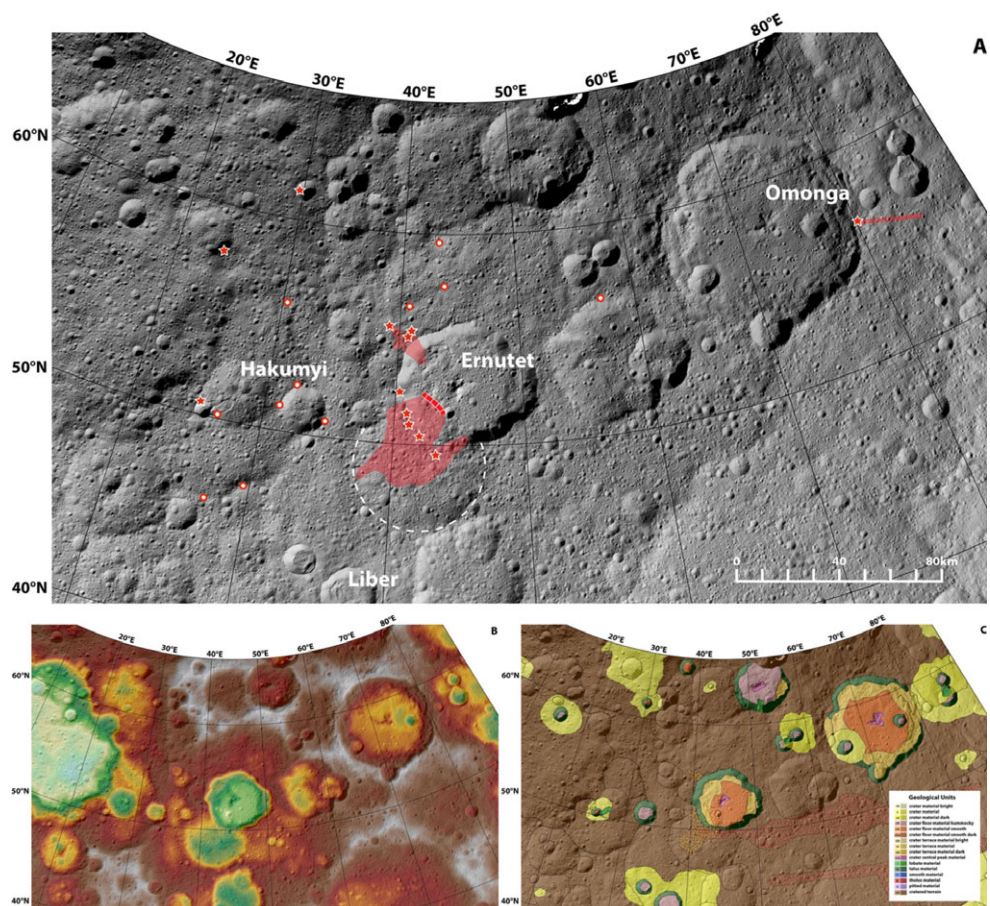
Fig. 1. Geologic context of the region on Ceres that exhibits organic material. A) Visible wavelength mosaic with red organic-rich (ROR) areas shown in red. Oversized stars are areas where the visible and infrared imaging spectrometer (VIR) identifies the presence of organics and the framing camera (FC) maps the extent. Stippled areas indicate broad ROR regions where surface features are diffuse or below the spatial resolution. Smaller red circles with white interior are where local areas are identified with the same properties in FC color data. The white dashed lines outline the approximate location of an older eroded crater. Basemap is a mosaic produced by Roatsch et al. (2016). B) Regional topography with more than 10 km relief, from yellow (low) to white (high). C) Regional geology as characterized by Pasckert et al. (2017). (Color figure can be viewed at wileyonlinelibrary.com.)

west of Ernutet on the rim of Hakumyi crater (29 km; ~51N°, 28°E), are estimated to be only ~30-50 Ma (LDM), and exhibit discrete ROR areas.

The sequence of pertinent cratering events in this region that excavated and redistributed material can thus be constructed to be the following. (1) As part of the evolving crust of Ceres, the old now heavily eroded unnamed 50 km crater southwest of Ernutet was formed. (2) The complex crater Ernutet formed substantially later partially obliterating portions of the eroded crater, and several sections of wall material were slumped onto floor material. (3) Impact cratering continued while craters as large as 4.6 km in diameter were formed on the floor of Ernutet. (4) The formation of a 6.5 km diameter crater occurred on the rim of Hakumyi crater, potentially associated with the

synchronous emplacement of a lobate flow deposit. Based on high-resolution images discussed below, emplacement or exposure of most or all of the ROR appears to have occurred much later than this sequence of events.

Long wavelength, HAMO spectral data acquired by VIR at ~390 m/pixel show no distinct thermal signature in the Ernutet area associated with the high density of ROR areas seen in Fig. 1A. This region, although slightly brighter than neighboring terrain, exhibits a surface temperature very similar to the surrounding terrain seen at the same local solar time and under comparable solar illumination. Therefore, at the several hundred meter scale, VIR thermal data detect no unusual regolith properties (compaction or particle size) associated with ROR terrain.

SPECTRAL PROPERTIES OF RED ORGANIC-RICH AREAS

Even with relatively low-resolution global FC color data, the Ernutet region was noticed as different from surrounding terrain and exhibited an unusually "red" overall continuum across the extended visible part of the spectrum (Nathues et al. 2016). An enhanced FC color image of this region acquired from the HAMO orbit is shown in Fig. 2. The unusual spectral properties are shown to be unevenly distributed across some of the floor and southwest wall of Ernutet including part of the heavily eroded crater to the south as well as a narrow zone along the northwest wall and exterior. Some areas, such as those indicated by the dark filled arrows, are small areas that exhibit intense spectral contrast, whereas broad diffuse areas exhibiting less color contrast are also observed.

The spectral properties of an example discrete red organic-rich area (ROR #1) and background Ceres are compared in Fig. 3 using both FC and VIR data. An average spectrum of Ceres (black) is dark and generally featureless across the visible and the near-infrared until beyond ~2.7 μm, where diagnostic features of hydrated silicates and ammoniated clays occur at 2.7 and 3.06 μm (De Sanctis et al. 2015). These two features occur everywhere across Ceres but with different strength, implying a common mineralogy of the surface but different local proportions (Ammannito et al. 2016). What distinguishes areas of ROR material across northern Ceres is the additional and prominent absorption at 3.4 μm along with a distinct continuum in the visible that is strongly sloped toward longer wavelengths (red). These coupled characteristics are illustrated in Fig. 4 where the spatial extent of areas with a prominent 3.4 μm absorption from VIR is spatially correlated with a distinctive red-sloped continuum measured by FC. Such properties of aliphatic organics (3.4 μm absorption band with prominent red-sloped continuum in the visible) is well documented in laboratory analyses of organic materials (Moroz et al. 1998). It is important to note, of course, that a red-sloped continuum is not unique to organics and can have other causes. Nevertheless, for areas on Ceres where the 3.4 μm organic absorption is demonstrated to be coupled to a red-sloped continuum, the higher spatial resolution FC color data can be used to evaluate the geologic context of the red organic-rich areas in finer detail. Shown in Fig. 5 is a comparison of seven-color FC spectra for several ROR areas found across the region. They are compared with background Ceres reference material and local young areas that exhibit a blue-sloped continuum. Although no diagnostic features are present at these short
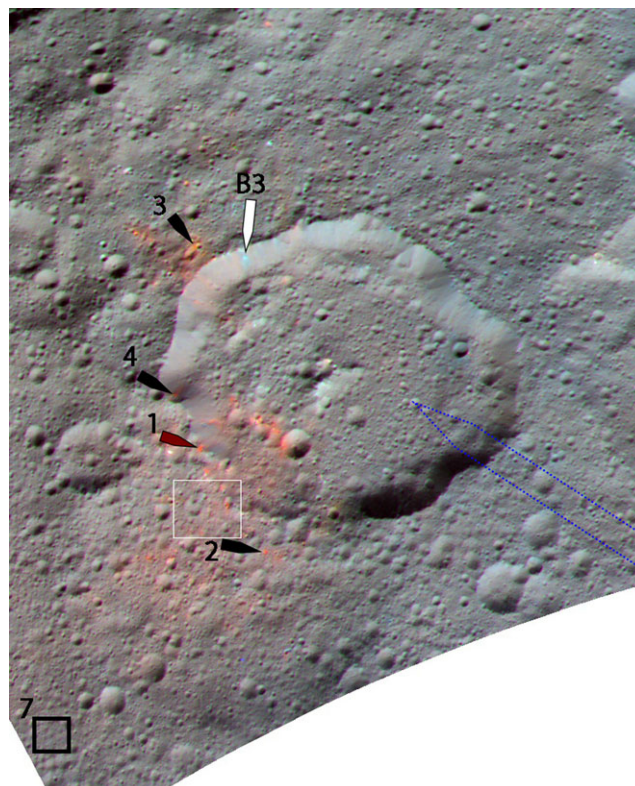

Fig. 2. Enhanced framing camera (FC) color image of the Ernutet area illustrating a concentrated distribution of ROR materials. In this HAMO image set, each channel is strongly contrast enhanced to emphasize small color variations with (R, G, B) = (960, 550, 440) nm. Location of several seven-band FC spectra that appear in Fig. 5 is indicated with symbols: Dark filled arrows indicate ROR areas 3, 4, 1, and 2; white arrow = area B3; black square = reference area 7. The white box indicates the area shown in Fig. 12. Broad blue arrow indicates the approximate viewing direction for Fig. 7. (Base figure after Schröder et al. [2017]; NASA PIA21419. This full image scene is available in Appendix S1 in supporting information). (Color figure can be viewed at wileyonlinelibrary.com.)

wavelengths, the distinct variations in continuum slope allow spectral and spatial relationships of surface materials to be evaluated in geologic context and at high spatial resolution.

LOCAL GEOLOGIC CONTEXT OF ROR MATERIALS

As illustrated in Fig. 4, areas of ROR materials identified as organic-rich by the 3.4 μm diagnostic absorption band in VIR data (Fig. 4C) also exhibit directly correlated variations across the visible continuum that are readily captured by a FC color ratio such as 960/440 nm (Fig. 4D). When such FC color data are acquired at higher spatial resolution, the spatial context of ROR can be more fully examined.
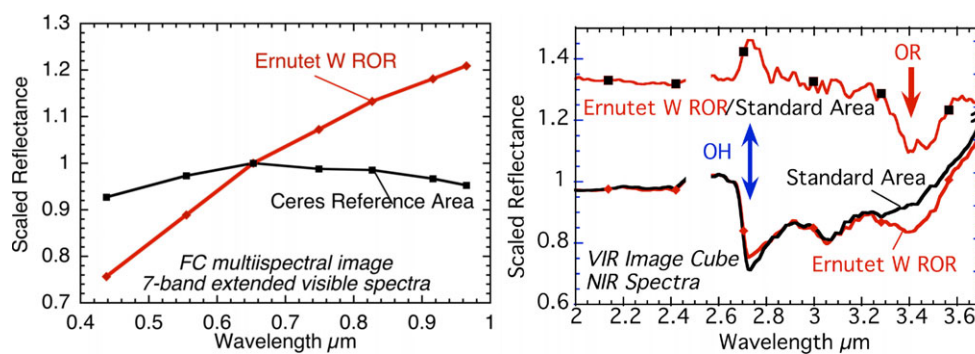
Fig. 3. Visible seven-color and near-infrared spectra acquired by FC and VIR for Ernutet west ROR area 1 (see Fig. 2 for location) compared with background Ceres material. Spectra are scaled to unity at a common wavelength to allow comparison of spectral features between ROR (red) and background Ceres (black). As VIR near-infrared spectra of Ceres contain several absorption features, a relative reflectance (ratio) spectrum of the ROR/Standard area allows the unique 3.4 μm feature of the organic-rich (OR) region to be clearly discerned. (Color figure can be viewed at wileyonlinelibrary.com.)

Global color mapping of Ceres was carried out during Dawn's HAMO orbits from an altitude of ~1470 km, with lesser amounts of color data obtained during the LAMO at ~380 km. LAMO science was optimized for gamma-ray and neutron detector (GRaND) chemistry measurements (Prettyman et al. 2017; Russell et al. 2016), and spacecraft motion at the lower altitude produced measurement challenges for optical instruments. Although both VIR and FC produce spectral data in an image (spatial) format, typical HAMO resolution for VIR at Ernutet is ~344 m/pixel and for FC is ~136 m/pixel. At LAMO, the FC resolution improves to ~35 m/pixel. The Ernutet region was identified as a high priority target for Dawn science and the Dawn flight team was able to acquire valuable high-resolution FC color data for several ROR targets during LAMO.

The geologic context characterized by these HAMO and LAMO color data for ROR materials is discussed below. Although the enhanced color image display of Fig. 2 allows color data to be readily examined in context visually, the standard process for producing such products requires several calibration and registration steps to be performed for each of three separate color images (filters) that were acquired sequentially and hence for slightly different areas on the surface. The necessary resampling during processing to coalign or register the images inevitably degrades the spatial resolution. Furthermore, terrain with high contrast (and shadows) at the pixel scale causes edge effects at such boundaries which are difficult to remove. Thus, procedures used to evaluate high-resolution images for spatial variations of color are chosen to minimize the resampling between images in order to maximize the spatial content. In the figures below, a ratio between two images widely spaced in wavelength is used to capture spatial variations of color across the

scene. The maximum color range (between 960 and 440 nm) is chosen for the ratio, such as is used as in Fig. 4D. In order to preserve the maximum spatial information for these analyses, most images have also not been resampled into the local coordinate system. All color data are derived from a single image sequence.

A HAMO color image set including the Ernutet–Hakumyi region is shown in Fig. 6. Topography variations disappear in a well-registered color ratio of two wavelengths (Fig. 6B) where illumination differences across the scene effectively cancel because illumination geometry is the same for each surface area in both filters. Only spatial variations in color should dominate a color ratio image (although a few residual artifacts remain in this scene at several sharp boundaries). Detailed spatial information for ROR materials found at different areas across the scene is seen in the color ratio image, in which bright indicates surface material with a strongly red-sloped continuum. As in Fig. 4, small discrete ROR areas are clearly identified. With modest processing (enhancement), nearby more diffuse and sometimes filamentary areas of ROR can be recognized. Many of the discrete areas and the diffuse areas are identified in both VIR and FC data. The discrete areas are displayed with oversized filled stars in Fig. 1A and the diffuse regions with stipple. Smaller areas with the same properties in FC images, and also presumed to be ROR, are scattered across the scene and are identified with small red circles with a white center. To avoid possible image-processing artifacts, only small areas with ROR properties that are verified in independent image sets are indicated in Fig. 1A.

Two concentrations of ROR materials identified near Ernutet by De Sanctis et al. (2017) include the large area across the floor and southwest wall and a smaller roughly triangular area extending from the
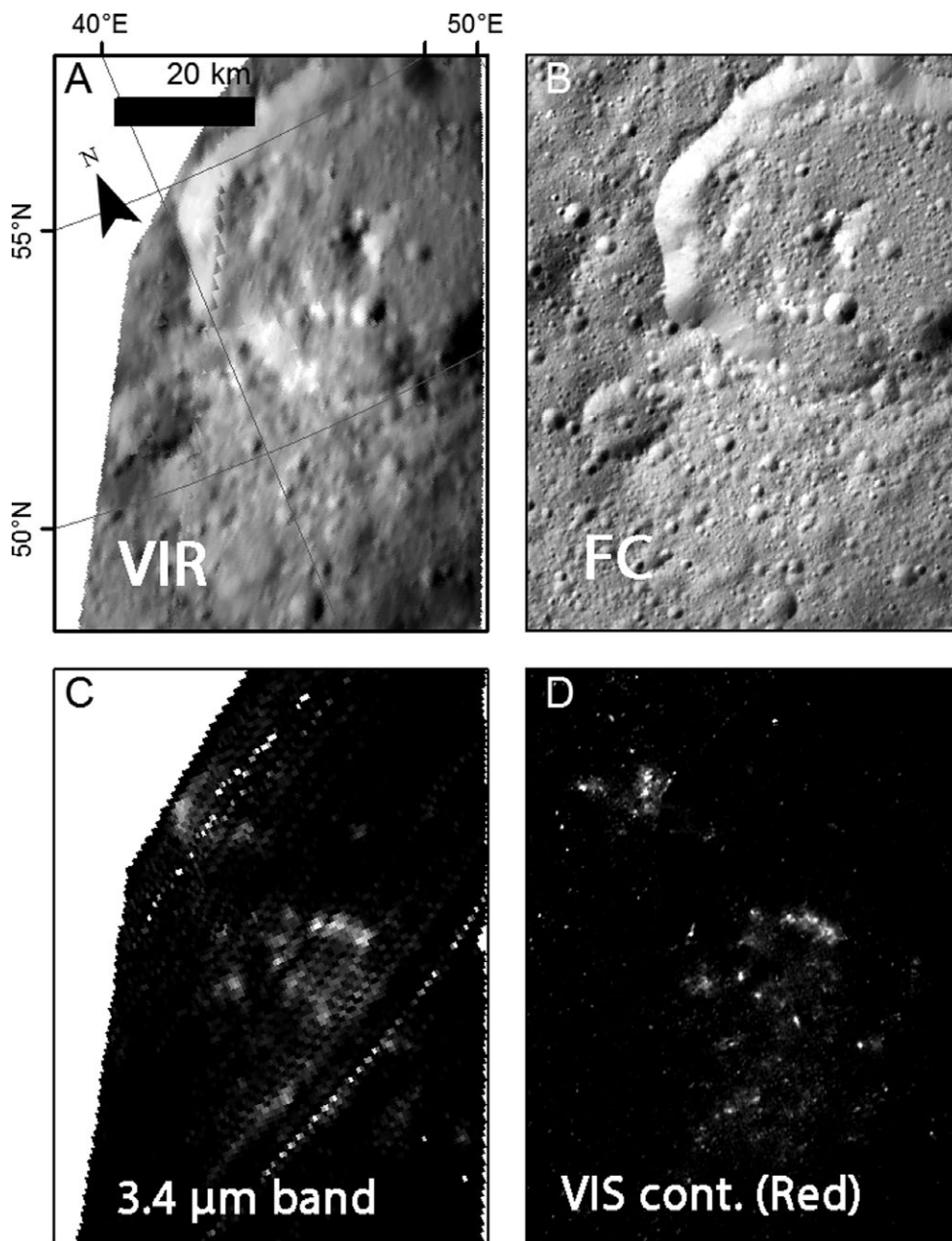
Fig. 4. Comparison of visible and near-infrared properties acquired across Ernutet with (A) the visible and near-infrared imaging spectrometer (VIR) and (B) the framing camera (FC) from the Dawn high-altitude mapping orbit (HAMO). The strength of the diagnostic 3.4 μm absorption band of organics measured by VIR (C) is spatially correlated with the steepness of the continuum across extended visible wavelengths (960/440 ratio) measured by FC (D).

northwest rim. These are readily seen in Fig. 6. Both are resolved into several smaller discrete ROR areas and diffuse regions between them with the higher resolution data. The loose talus found along the wall of Ernutet corresponds to recent small impact events with down-slope movement. The oblique view of enhanced color superimposed on a derived digital terrain model of Ernutet shown in Fig. 7 suggests that a greater

number of recent small impacts affected the talus along the part of Ernutet crater wall (which exhibits a ROR cluster just beyond the rim as seen in Fig. 2).

The lower left corner of the image set in Fig. 6 includes two discrete ROR areas found along the rim of Hakumyi (Figs. 6B and 6C). An additional HAMO image sequence of ROR material at Hakumyi is shown in Fig. 8. Although no color data for this area were
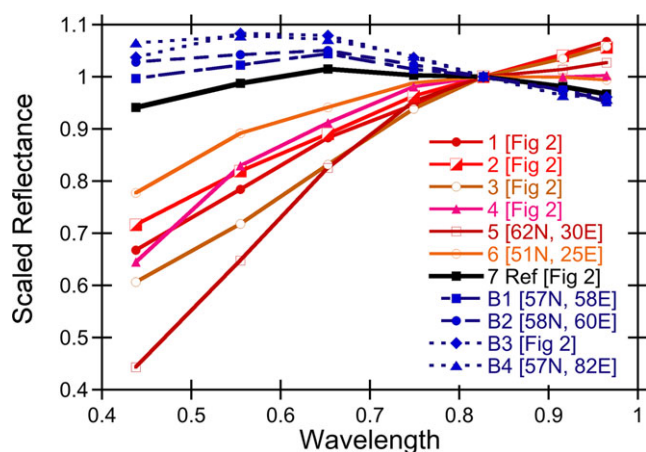
Fig. 5. Example seven-band spectral properties measured by FC for regions identified by VIR as containing the diagnostic 3.4 μm absorption signature for organics. Spectra 1, 2, 3, and 4 correspond to local organic-rich concentrations mapped by De Sanctis et al. (2017) in their area "A" associated with southwest Ernutet (see Fig. 2), spectrum 5 corresponds to concentrations identified at their area "E," and spectrum 6 corresponds to their area "C." For comparison are a reference spectrum typical of average Ceres (7) and several other nearby spectra that exhibit a distinctively blue-sloped continuum (B1–B4). Spectra are scaled at band 820 nm for ease of comparison. (Color figure can be viewed at wileyonlinelibrary.com.)

acquired during LAMO, multiple images of LAMO clear filter data were obtained at ~35 m/pixel providing high-resolution information to characterize local morphology. Discrete ROR areas are associated with the relatively young 6.5 km crater on the rim of Hakumyi. Two ROR areas are found along the northern rim, one of which (black or gray arrows) is associated with two to three very small craters (<100 s m in size) found on a small plateau and the other found in areas of nearby talus. This area was clearly identified by its prominent organic 3.4 μm absorption in VIR data (De Sanctis et al. 2017). In addition, the image data clearly identify the properties of a small elongated ROR area (white arrows) along the edge of the lobate flow associated with the crater. These ROR areas are also seen in the independent data shown in Fig. 6. While the estimated age of the 6.5 km crater and the adjacent lobate flow is ~30–50 Ma, superposition relations indicate that the exposure and/or emplacement of ROR material in this area is distinctly younger, although the absolute age is unknown.

High-resolution color data from LAMO orbit were obtained for a few regions containing ROR. Two examples are shown in Figs. 9 and 10 covering the floor and southwest wall of Ernutet. ROR material that is seen with the group of medium-sized craters on the floor in HAMO data (Fig. 6) is resolved into discrete small areas interspersed among the larger floor craters in an approximate linear manner apparently unrelated to the floor craters. Because the image sets for Figs. 9 and 10 are completely independent, they can be used to validate the highly discrete nature of several small ROR. The small streak of ROR material along the edge of a crater in the upper right corner of Fig. 9B (red arrow) is confirmed in lower resolution HAMO data.

The southwest rim of Ernutet shown in Fig. 10 appears relatively coherent and exhibits small impact craters. The high spatial resolution LAMO data allow a clear association of ROR areas to be identified with very small, recent craters. Two such craters readily identified in Fig. 10 (arrows) correspond to discrete ROR areas seen in both VIR and FC spectral data. These are identified as ROR areas 1 and 4 in Figs. 2, 3, and 5. A zoom of the small crater at area 1 (for which full spectra are shown in Fig. 3) is presented in Fig. 11. Although distinct, the crater is barely resolvable with LAMO resolution (36 m/pixel), indicating the crater is only a few hundred meters in diameter. If the exposures of ROR material along the floor are also from small fresh craters, as appears likely, the craters themselves are smaller than the 36 m resolution of LAMO data.

The easternmost ROR area identified by De Sanctis et al. (2017) is found near the rim of Omonga. Although no LAMO color data are available for this site, LAMO clear filter images are available and allow the morphology and geologic context of the ROR area to be evaluated. HAMO color data shown in Fig. 12 coupled with LAMO clear filter data (Appendix S1) indicate that the VIR ROR site is centered on a small recent crater with a faint long relatively linear trail of similar material extending to the east. The Omonga region exhibits many optical properties of typical craters found on Ceres. For example, the 11 km crater to the west of Omonga between two white arrows is young (~13 Myr; Pasckert et al. 2017) and exhibits a relatively blue-sloped continuum (B1 and B2 in Fig. 5) common to large fresh craters on Ceres (Schmedemann et al. (2016). The ~10 km fresh crater, a few km to the northeast of the ROR site, also exhibits a small zone of blue-sloped material (B4), apparently the result of a small impact onto its rim (also see Fig. F6 in Appendix S1).

Even though LAMO color data do not provide global coverage and individual image sets retain processing artifacts due to the sequential nature of their acquisition, the results have been most helpful in evaluating the geologic context of ROR materials. An example of the difference that high-resolution spatial information provides can be seen in HAMO–LAMO comparison of the same area shown in Fig. 13. The
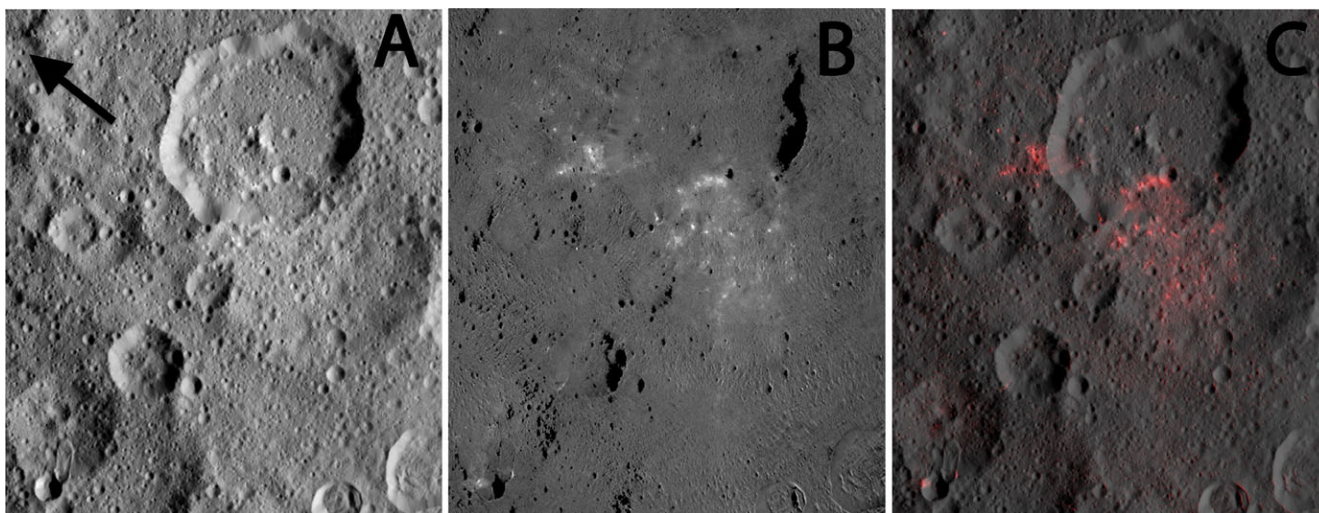
Fig. 6. HAMO FC image set across the Ernutet–Hakumyi region. Black arrow points north. A) 960 nm [image FC21B0045375 filter 5]. B) Color ratio: 960/440 nm, stretched 0.40–0.62. C) Composite image of red 960/440 nm color ratio contrast enhanced and superimposed on 960 nm brightness with 50% opacity. Deep shadows have been masked for the color ratio images. Edge effect artifacts can be seen in parts of the color ratio, especially in the lower right of the image. This image sequence is independent of that in Figs. 2 and S1 in Appendix S1. (Color figure can be viewed at wileyonlinelibrary.com.)
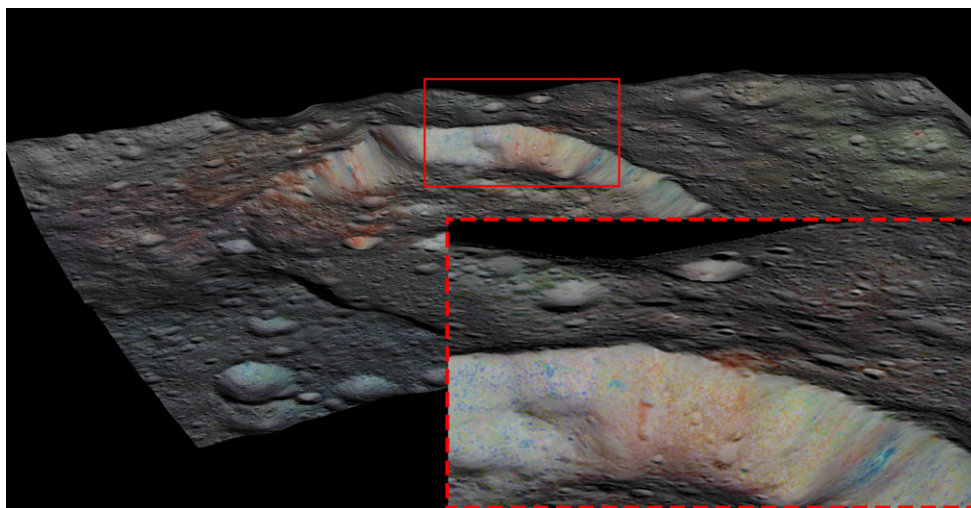

Fig. 7. Enhanced color superimposed on a digital terrain model for Ernutet crater. Viewing direction is shown on Fig. 2. An enlargement of the northwestern rim highlights an apparent higher density of recent impacts into the wall talus below a cluster of ROR just beyond the rim. An alternate version with LAMO color composite data is available in Fig. S2 in Appendix S1. (Color figure can be viewed at wileyonlinelibrary.com.)

small ROR area near the bottom of the image is seen as a blur in HAMO resolution, but is clearly shown to be associated with a small crater (arrow) at LAMO resolution. On the other hand, the ROR area seen in the middle right of the scene at low resolution appeared to be linked to a crater within a crater, while the higher resolution data suggest that is not the case, although the specific local morphology remains undefined.

INTEGRATED OBSERVATIONS AND IMPLICATIONS

The above examples illustrate that discrete ROR areas identified on Ceres are closely tied to recent very small impact events, some of which are below Dawn's LAMO FC resolution (35 m/pixel). In addition, terrain with a high density of discrete ROR areas (e.g., near
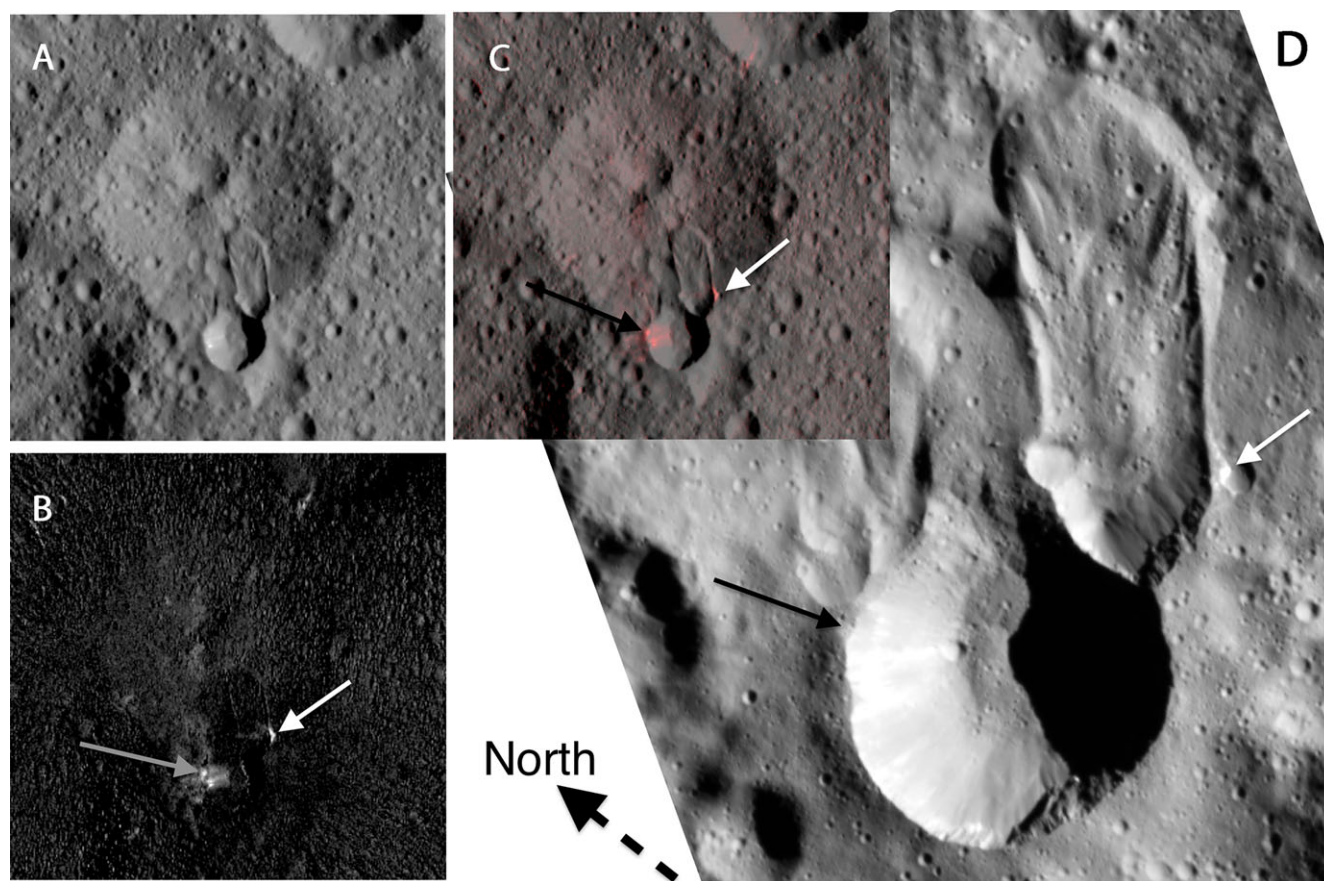
Fig. 8. ROR areas associated with a 6.5 km young crater and lobate flow along the rim of Hakumyi. Dashed arrow indicates north direction. These data are from a HAMO image set independent from that of Fig. 6. A) 960 nm brightness image [FC21B0039995 Filter 5]. B) 960/440 nm color ratio, enhanced. C) Composite image of color ratio in red superimposed on 960 image with 50% opacity. D) LAMO clear filter image FC21B0057743. White arrows and black+gray arrows indicate the same locations in each image. The orientation of the triangular ROR area visible in B, C, and D suggests an oblique impact. A closer view is shown in as Fig. S3 in Appendix S1. (Color figure can be viewed at wileyonlinelibrary.com.)

Ernutet) also exhibits a background of diffuse ROR material. Resolvable craters associated with ROR material are no larger than a few hundred meters in diameter. With only one apparent exception, all of the ROR areas are found across a ~200 km elongated region on northern Ceres shown in Fig. 1A. Except for the cluster of ROR areas near Ernutet (including related talus movement down slopes), most occurrences of ROR materials are widely separated, discrete, and quite small. A few instances suggest possible directionality, implying oblique impact for the small craters associated with ROR material (e.g., along the lobate flow at Hakumyi [Fig. 8], the trail at Omonga [Fig. 12], the thin streak in northeast Ernutet [Fig. 9], and perhaps a concentration of features in northwest Ernutet talus [Fig. 7]). Although no regular pattern has been identified, an approximate direction could be that of the blue arrow in Fig. 2 (the view from Fig. 7), which roughly aligns with the elongated distribution of ROR material in Fig. 1A.

Although it might be reasonable to assume that ROR areas all have a common origin, there is currently no explicit rationale to support the assumption.

Independent of the origin of the ROR material, the clear geologic association with small craters indicates the organic material is distinctly near-surface on Ceres. The discrete and highly localized nature of ROR material and the limited size of associated craters (Figs. 8, 9, 10, and 12) place it only within the upper few tens of meters. Although the small craters must be relatively recent, there is currently insufficient information to estimate age or even whether later events occurred after their formation. Regardless, the analysis of geologic context from all data available indicates that either the exposure of pre-existing material (endogenic) or the emplacement of concentrated ROR materials (exogenic) is recent.

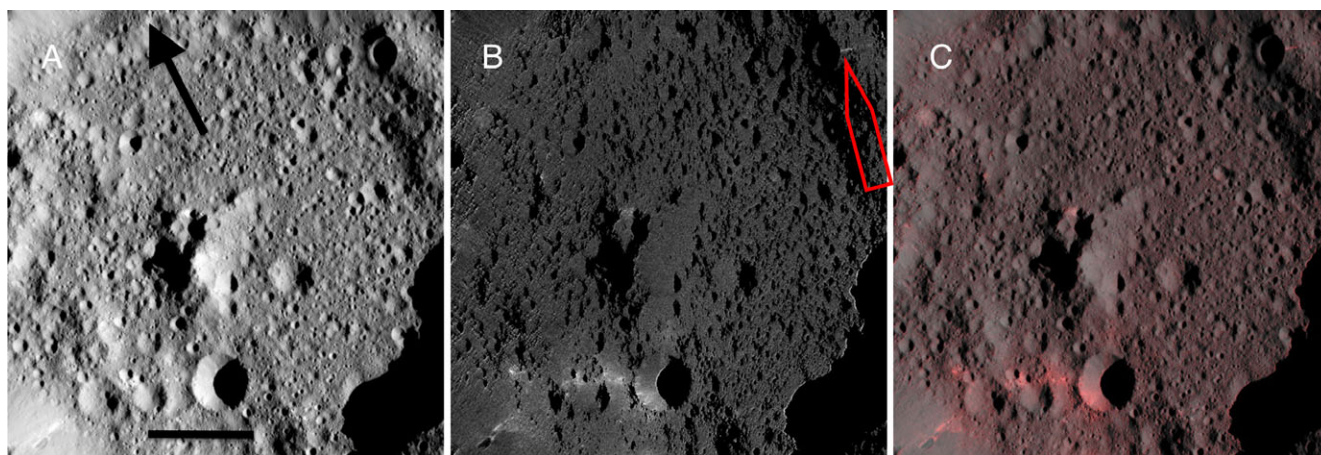The overall pattern observed for ROR areas in Fig. 1A and the association with very small fresh

Fig. 9. LAMO image set covering the floor of Ernutet. A) 960 nm brightness image (black arrow indicates north; scale bar is 10 km). B) 960/440 nm color ratio image. C) Composite image of color ratio 960/440 in red superimposed on 960 nm image with 50% opacity. Several of the color features in the lower part of the image are below the LAMO resolution (36 m/pixel). The small ~linear color streak in the upper right of (B) (red arrow) is confirmed in independent images. Full resolution images are provided in as Fig. S4 in Appendix S1. (Color figure can be viewed at wileyonlinelibrary.com.)
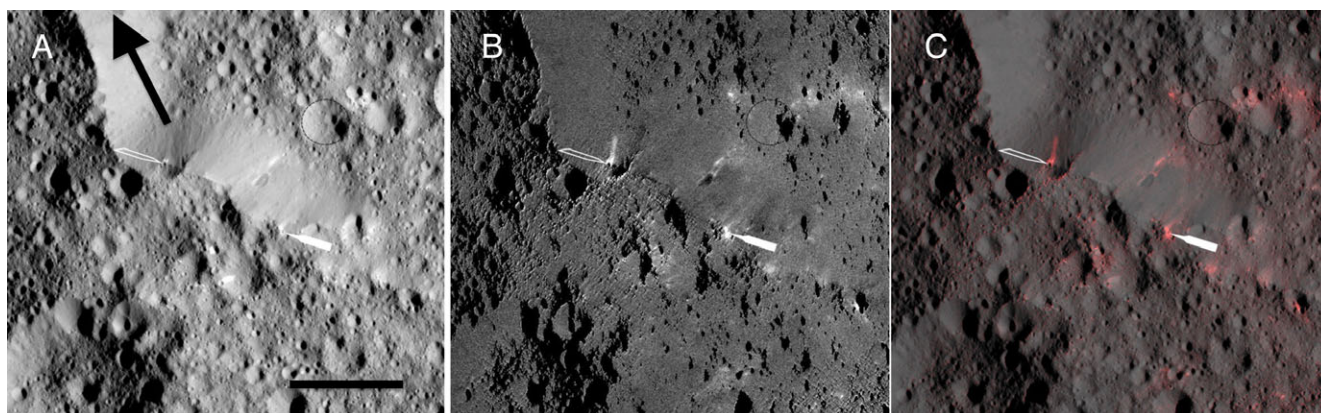

Fig. 10. LAMO image set along the rim of Ernutet (overlaps with the lower part of Fig. 9). Unfilled arrow indicates area 4; Filled arrow is area 1. Lightly dished circles outline a few floor craters. A) 960 nm brightness image (black arrow indicates north; scale bar is 10 km). B) 960/440 nm ratio image. C) Composite image of red color ratio 960/440 superimposed on 960 image with 50% opacity. In both areas, the strong ROR signature is associated with a small recent crater. Full-resolution images are provided in as Fig. S5 in Appendix S1. (Color figure can be viewed at wileyonlinelibrary.com.)

craters could be consistent with a field of secondary craters, as has been observed on the Moon and Mars (e.g., McEwen et al. 2005; Dundas and McEwen 2007) that might have been produced by a recent large impact elsewhere on Ceres. This could provide an attractive scenario that would enable bringing deeper crustal material to the surface as the lower velocity of secondary impacts would allow more of the material from the source crater to be retained as a surface component (e.g., Daly and Schultz 2015). Deposition and mixing of significant amounts of nonlocal material far from the source crater has been well modeled and documented in the lunar case (Oberbeck 1975; Pieters et al. 1985; Hawke et al. 2004). Although models exist to predict the distribution of crater ejecta and rays across Ceres (e.g., Schmedemann et al. 2017), no viable recent source crater for ROR materials has been identified and, equally important, no intermediate or large crater exhibiting distinct organic signatures in the visible or near-infrared is found on Ceres. Either such a source crater for the organics does not exist or its properties have been altered with time to be unrecognizable, and the small fresh ROR craters thus have a different source.

Although the geologic context of organic-rich material found on Ceres is now relatively well defined, the origin of these most interesting materials remains somewhat ambiguous. Shown in Fig. 14 are possible cross sections for a small crater in the Ernutet region (panels A and B) and a smaller crater near Hakumyi
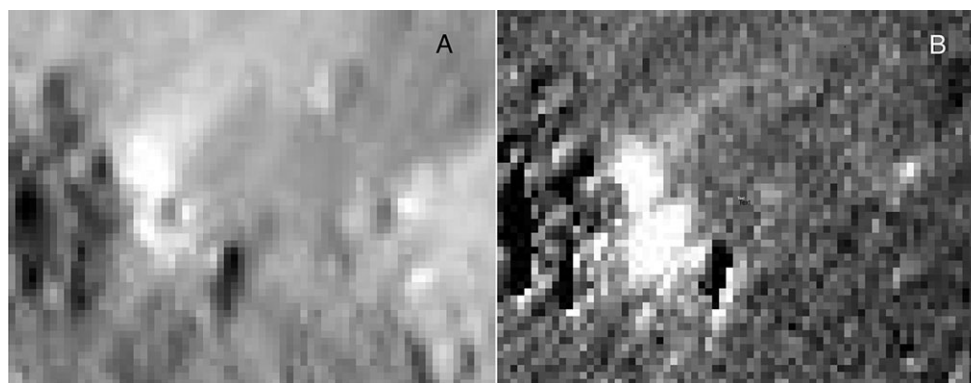
Fig. 11. LAMO zoom images of area 1, filled arrow in Fig. 10. Resolution is 36 m/pixel. A) 960 nm brightness. B) 960/440 nm ratio image (bright indicates red-sloped continuum). The small crater associated with the discrete ROR material is 3–6 pixels in diameter, or 100–200 m. The dark region in lower center is a deep shadow, which is largely masked in the ratio image.
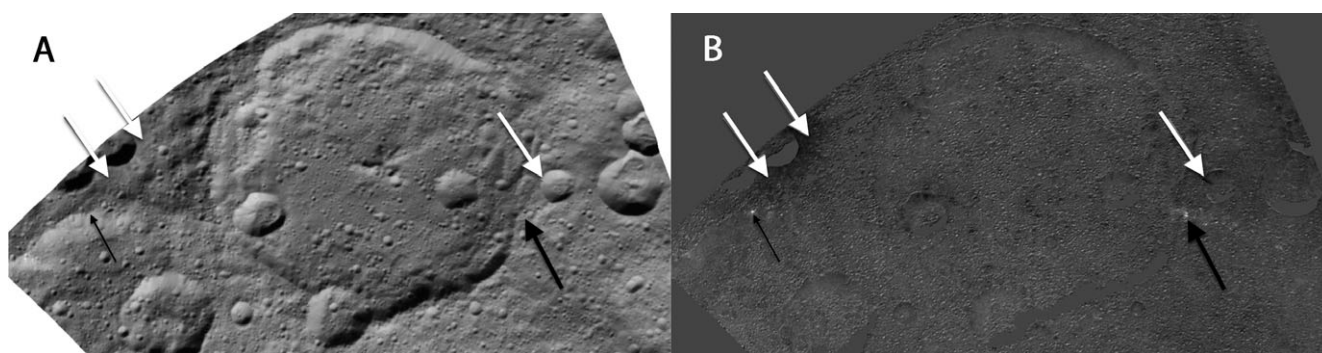

Fig. 12. Projected HAMO data for the Omonga region with north toward the top. A) Brightness 960 nm image. B) Color ratio 960/440 nm. White arrows (low values of ratio) indicate location of areas B1, B2, and B4 (left to right) for spectra in Fig. 5. The easternmost ROR area from De Sanctis et al. (2017) is indicated with a large black arrow. A faint trail of similar material can be seen extending to the east. The small black arrow indicates a small discrete area with ROR properties. A coordinated clear filter LAMO image of the eastern ROR region is provided in as Fig. S6 in Appendix S1.

(panels C and D) which result in ROR material on the surface. Panels A and C could represent recent delivery of ROR material from an external source and B and D could represent exposure of ROR materials on the surface from pre-existing material. Given the extended geologic history of the region, the pre-existing material would most likely be the product of past, perhaps ancient, event(s) such as deep-seated deposits from a major impact or extrusions from internal processes. In this schematic figure, the discrete small craters (less than a few hundred meters) of ROR material in the Ernutet region could result from either (A) local impactor contamination associated with the crater or (B) excavation of near-surface ROR material of unknown thickness. The regolith of the diffuse ROR region observed near Ernutet (pink in A and B) results either from (A) accumulation and mixing of abundant organic-bearing small debris arriving with the larger object forming the crater or (B) regolith gardening and mixing of near-surface organic-rich material. On the other hand, the ROR material near Hakumyi (panels C and D) is representative of the widely dispersed discrete areas of ROR material shown in Fig. 1A. These are small areas of distinct ROR material surrounded by typical material found elsewhere across Ceres. In (C), the ROR material results from contamination by an impacting body (in this case from a somewhat oblique direction), whereas in (D), the observed ROR material is derived from an isolated small block of pre-existing ROR material located near the surface at the impact point. Note that while the lower panels involving pre-existing ROR material (B and D) would most likely represent products of endogenic processes on Ceres, they could also conceivably represent ancient ROR deposits from a major impact with an organic-rich body (similar to the model for Vesta's concentration of water from exogenic carbonaceous chondrite material [Prettyman et al. 2012; De Sanctis et al. 2012]).

Determining the origin of the prominent organic material found on Ceres is not simple. Challenges with
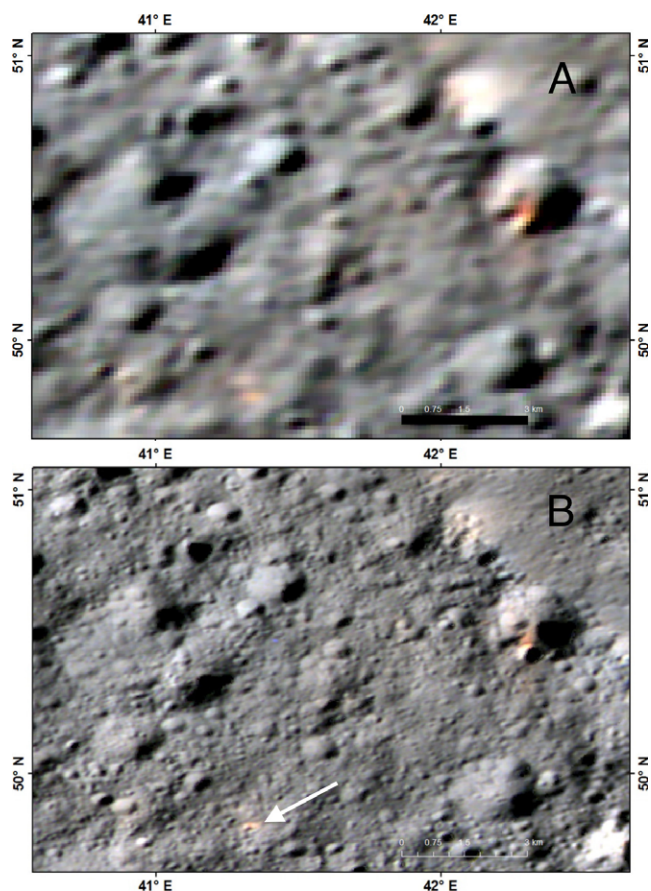
Fig. 13. Comparison of FC-enhanced color for the same region acquired during the HAMO (A) and LAMO (B). Scale bar is 3 km. Enhancement is less than that of Fig. 2 to better discern local morphology. The association with very small craters (arrow) and discrete nature of many ROR areas is apparent in the high-resolution LAMO data (35 m/pixel). (Color figure can be viewed at wileyonlinelibrary.com.)

both the endogenic and the exogenic hypotheses need further analyses to be resolved.

Endogenic Origin

An endogenic origin requires (1) a mechanism to produce material enriched in aliphatic organics within Ceres and then (2) transportation of the organics to the near-surface. Both parts of the problem can be solved (production and transport), but identifying an integrated solution is presently elusive. The production of organic material in Ceres' interior during its history of extended aqueous alteration (e.g., Castillo-Rogez et al. Forthcoming, 2018) is quite viable. Processes to bring the ROR material to the surface in the patterns observed are more problematic.

At Ernutet's high latitude, the cold surface environment inhibits material upwelled from the interior

to progress to the surface. Excavation, deposition, and mixing by impact processes are the more likely processes for material transport. At HAMO and lower resolution, the northwest and southwest distribution of ROR materials around Ernutet suggests excavation and exposure of subsurface organic material during the Ernutet impact. In support of this hypothesis, the distribution appears similar to materials observed at a similar size but much younger crater on Ceres, Azacca (7S, 218E). Although quite different in age and composition, these presumed ejecta deposits of Azacca (see Fig. S7 in Appendix S1) exhibit a high density of distinct small bright areas that have been tentatively interpreted to be concentrations of crustal components excavated and dispersed during the Azacca impact.

However, integrated data from the high-resolution LAMO data reveal issues that make Ernutet itself less likely as a source crater for ROR materials. For example, the discrete pattern of ROR across the surface of Ernutet floor is difficult to produce through excavation of interior ROR by the original Ernutet impact. Floor materials in such complex craters normally are a mixed and brecciated product of the impact debris, also often containing melt material from the impact. Several kilometer-sized craters that formed later (Figs. 9 and 10) continued to rearrange and mix Ernutet floor materials to depths of several hundred meters. The array of discrete ROR seen across the floor's surface is distinctive and appears in an approximately linear pattern that is indiscriminant of these older kilometer-sized craters. Such a pattern is highly unlikely to have been retained through the formation and extended impact history of floor material.

The small craters associated with distal discrete ROR areas are recent (e.g., Figs. 8 and S3 in Appendix S1) and obviously not directly derived from Ernutet (~1.6 Ga). For the non-Ernutet ROR materials to be derived from Ernutet, they would need to have been excavated and emplaced (at 1.6 Ga) in the near-surface as coherent blocks of ROR material large enough to be later re-excavated and exposed by a small crater.

Exogenic Origin

An exogenic origin requires both (1) an external organic-rich source that resides in or passes through the main asteroid belt to interact with Ceres and (2) preservation of detectable amounts of organics during the interaction. Evaluating sources of organics in the solar system is currently data limited. As mentioned in the Introduction, identification of organic-rich material has been successful for a few instances, largely in the outer solar system, and organics are also even suspected
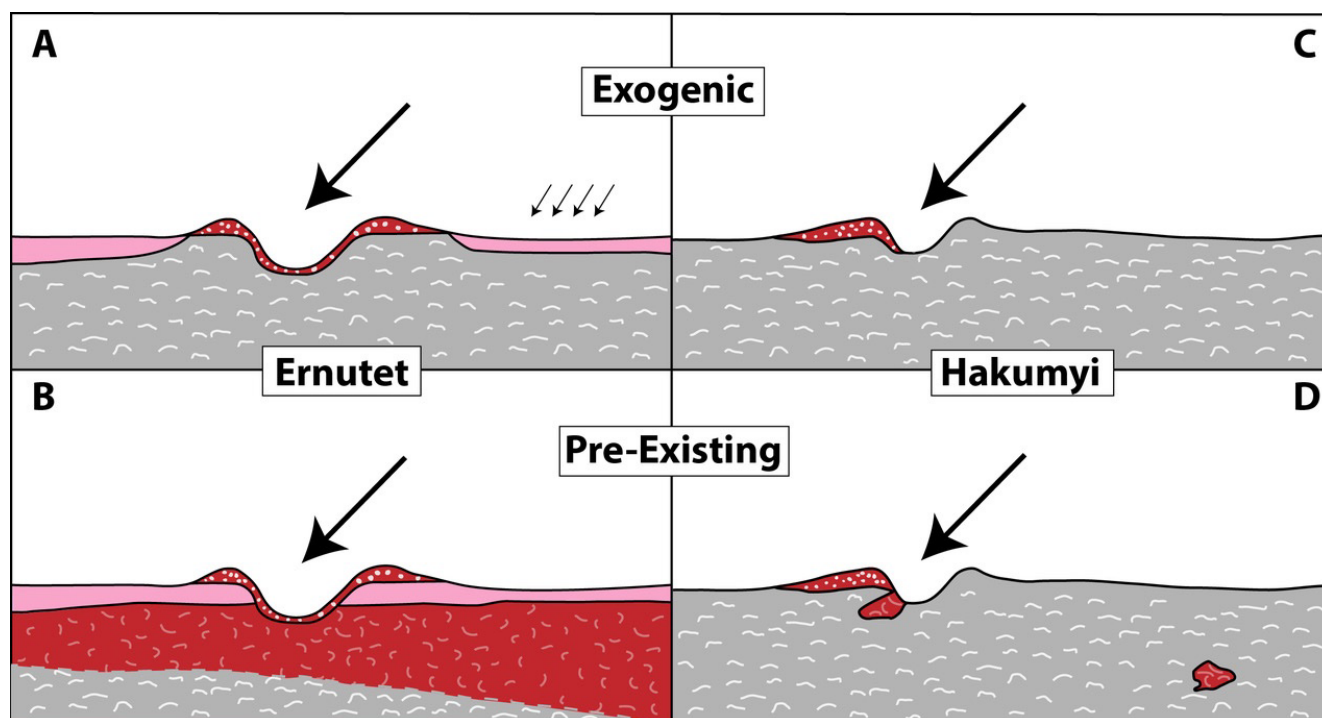
Fig. 14. Schematic cross section across red organic-rich material (ROR) areas in Ernutet (A and B) and near Hakumyi (C and D). Each panel depicts a small crater event associated with discrete ROR of the area. The upper panels (A and C) represent ROR material delivered from an external source and the lower panels (B and D) represent exposure of ROR material from pre-existing material. ROR material is shown as red, regolith with abundant ROR as pink, and typical Ceres as gray. (Color figure can be viewed at wileyonlinelibrary.com.)

of accumulating in the protected poles of the innermost planet, Mercury (Paige et al. 2013). For Ceres, if the geometry is right or the velocity is relatively low, impact physics predicts a substantial component of an impactor to be retained (Daly and Schultz 2015).

Debris of all kinds, forms, and sizes moves across the solar system, only some of which we can observe or sample. Currently, our only documented extraterrestrial samples are from the Moon, near-Earth asteroid Itokawa, and dust from comet Wild 2. All other samples arrive as meteorites that are strong enough to survive passage through the Earth's atmosphere and are thus highly biased toward coherent materials. We have very little direct experience with underdense solar system materials.

Modeling impacts and their effects normally focuses on a singular event and its products, which is amenable to predictions by varying velocity, mass, composition, geometry, etc. for both the target and impactor. Because their physical properties are poorly defined, however, low strength or highly porous materials (both target and impactor) have typically not been fully analyzed. Nevertheless, experiments with very low density or dispersed cluster of impactors demonstrate that the amount of material retained is relatively high

and the shape of resulting craters differs appreciably from craters formed in more coherent materials (Schultz and Gault 1985).

Furthermore, from recent Vesta analyses (and previous studies of howardites), it is now known that exogenic materials are indeed retained on an asteroid surface (e.g., De Sanctis et al. 2012; Prettyman et al. 2012; Reddy et al. 2012). Nevertheless, a key issue facing an origin of ROR as debris from an exogenic source is that material leaving a comet, asteroid, or other solar system body is expected to disperse during its travel to Ceres (e.g., Sykes et al. 1986) and is unlikely to produce the observed localized 200 km field of ROR materials.

Other

If neither of the above options prove to be viable, alternate mechanisms might be investigated to produce the observed organics on Ceres. For example, are there conditions that would allow a small body of known material impacting onto Ceres to create the appropriate organic species in situ (e.g., McKay and Borucki 1997)? Similarly, if the very small craters are special and are the most recent events exposing fresh crustal components of Ceres, is ROR material created on a regular basis by

impacts only to be later altered and mixed into the regolith?

CONCLUDING REMARKS AND FUTURE INVESTIGATIONS

Ceres presents a wonderful natural laboratory involving organic species in our solar system. Dawn has provided two substantial new pieces of information that bear on the origin and evolution of life: the clear detection and characterization of aliphatic organics across parts of the surface of Ceres (De Sanctis et al. 2017), and the geologic constraints under which these organics occur (this work). Samples of solar system organics have been documented in tiny interplanetary dust particles (Flynn et al. 2003) and in samples returned from comet Wild 2 (Sandford et al. 2006). Although organics are found in samples of primitive meteorites (e.g., Pizzarello et al. 2006; Takir et al. 2013), meteorites in our collections clearly represent a biased sample of materials that are strong enough to survive entry through the atmosphere to be collected on the Earth's surface. The most friable organic-rich material that currently exists in the solar system is thus most likely missing from our sample collection. Properties of such material might be inferred from the clues we have with samples in hand or from possible links to the interstellar medium (Pendleton and Allamandola 2002).

The organics that occur on the surface of Ceres are very prominent and provide an important clue for the origin and evolution of organics across the solar system. The Ceres organics were either created in the interior or on the surface of this dwarf planet or were brought to the surface recently by a (presumably) common source which exists in that part of the solar system. In either case, these integrated Dawn data from Ceres present valuable information that require new insight and directions of inquiry concerning solar system organics as well as opportunities for a deeper understanding as exploration continue in the years ahead.

Editorial Handling—Dr. Hap McSween

REFERENCES

Ammannito E., DeSanctis M. C., Ciarniello M., Frigeri A., Carrozzo F. G., Combe J.-P., Ehlmann B. L., Marchi S., McSween H. Y., Raponi A., Toplis M. J., Tosi F., Castillo-Rogez J. C., Capaccioni F., Capria M. T., Fonte S., Giardino M., Jaumann R., Longobardo A., Joy S. P., Magni G., McCord T. B., McFadden L. A., Palomba E., Pieters C. M., Polanskey C. A., Rayman M. D., Raymond C. A., Schenk P. M., Zambon F., and Russell C. T. 2016. Distribution of phyllosilicates on the surface of Ceres. *Science* 353:aaf4279.

Capaccioni F., Coradini A., Filacchione G., Erard S., Arnold G., Drossart P., De Sanctis M. C., Bockelee-Morvan D., Capria M. T., Tosi F., Leyrat C., Schmitt B., Quirico E., Cerroni P., Mennella V., Raponi A., Ciarniello M., McCord T., Moroz L., Palomba E., Ammannito E., Barucci M. A., Bellucci G., Benkhoff J., Bibring J. P., Blanco A., Blecka M., Carlson R., Carsenty U., Colangeli L., Combes M., Combi M., Crovisier J., Encrenaz T., Federico C., Fink U., Fonti S., Ip W. H., Irwin P., Jaumann R., Kuehrt E., Langevin Y., Magni G., Mottola S., Orofino V., Palumbo P., Piccioni G., Schade U., Taylor F., Tiphene D., Tozzi G. P., Beck P., Biver N., Bonal L., Combe J.-P., Despan D., Flamini E., Fornasier S., Frigeri A., Grassi D., Gudipati M., Longobardo A., Markus K., Merlin F., Orosei R., Rinaldi G., Stephan K., Cartacci M., Cicchetti A., Giuppi S., Hello Y., Henry F., Jacquinod S., Noschese R., Peter G., Politi R., Reess J. M., and Semery A. 2015. The organic-rich surface of comet 67P/Churyumov-Gerasimenko as seen by VIRTIS/Rosetta. *Science* 347:aaa0628.

Castillo-Rogez J. C. and McCord T. B. 2010. Ceres evolution and present state constrained by shape data. *Icarus* 205:443–459. https://doi.org/10.1016/j.icarus.2009.04.008

Castillo-Rogez J. C., Neveu M., McSween H. Y., Fu R., Toplis M., and Prettyman T. Forthcoming, 2018. Insights into Ceres' evolution from surface composition. *Meteoritics & Planetary Science*.

Cruikshank D. P. 1997. Organic matter in the outer solar system: From the meteorites to the Kuiper Belt. In *From Stardust to Planetesimals*, edited by Pendleton Y. J. and Tielens A. G. G. M. *ASP Conference Series* 122:315–333.

Daly R. T. and Schultz P. H. 2015. Predictions for impactor contamination on Ceres based on hypervelocity impact experiments. *Geophysical Research Letters* 42:7890–7898.

De Sanctis M. C., Coradini A., Ammannito E., Filacchione G., Capria M. T., Fonte S., Magni G., Barbis A., Bini A., Dami M., Ficai-Veltroni I., and Preti G. 2011. The VIR spectrometer. *Space Science Reviews* 163:329–369.

De Sanctis M. C., Combe J.-P., Ammannito E., Palomba E., Longobardo A., McCord T. B., Marchi S., Capaccioni F., Capria M. T., Mittlefehldt D. W., Pieters C. M., Sunshine J., Tosi F., Zambon F., Carraro F., Fonte S., Frigeri A., Magni G., Raymond C. A., Russell C. T., and Turrini D. 2012. Detection of widespread hydrated materials on Vesta by VIR imaging spectrometer on board the Dawn mission. *Astrophysical Journal Letters* 758:L36.

De Sanctis M. C., Ammannito E., Raponi A., Marchi S., McCord T. B., McSween H. Y., Capaccioni F., Capria M. T., Carrozzo F. G., Ciarniello M., Longobardo A., Tosi F., Fonte S., Formisano M., Frigeri A., Giardino M., Magni G., Palomba E., Turrini D., Zambon F., Combe J.-P., Feldman W., Jaumann R., McFadden L. A., Pieters C. M., Prettyman T., Toplis M., Raymond C. A., and Russell C. T. 2015. Ammoniated phyllosilicates with a likely outer solar system origin on (1) Ceres. *Nature* 528:241–244.

De Sanctis M. C., Raponi A., Ammannito E., Ciarniello M., Toplis M. J., McSween H. Y., Castillo-Rogez J. C., Ehlmann B. L., Carrozzo F. G., Marchi S., Tosi F., Zambon F., Capaccioni F., Capria M. T., Fonte S., Formisano M., Frigeri A., Giardino M., Longobardo A., Magni G., Palomba E., McFadden L. A., Pieters C. M., Jaumann R., Schenk P., Mugnuolo R., Raymond C. A., and Russell C. T. 2016. Bright carbonate deposits as evidence of aqueous alteration on (1) Ceres. *Nature* 536:54–57.

De Sanctis M. C., Ammannito E., McSween H. Y., Raponi A., Marchi S., Capaccioni F., Capria M. T., Carrozzo F. G., Ciarniello M., Fonte S., Formisano M., Frigeri A., Giardino M., Longobardo A., Magni G., McFadden L. A., Palomba E., Pieters C. M., Tosi F., Zambon F., Raymond C. A., and Russell C. T. 2017. Localized aliphatic organic material on the surface of Ceres. *Science* 355:719–722.

Dundas C. M. and McEwen A. S. 2007. Rays and secondary craters of Tycho. *Icarus* 186:31–40.

Flynn G. J., Keller L. P., Feser M., Wirick S., and Jacobsen C. 2003. The origin of organic matter in the solar system: Evidence from the interplanetary dust particles. *Geochimica et Cosmochimica Acta* 67:4791–4806.

Hawke B. R., Blewett D. T., Lucey P. G., Smith G. A., Bell J. F. III, Campbell B. A., and Robinson M. S. 2004. The origin of lunar crater rays. *Icarus* 170:1–16.

Hendrix A. R., Vilas F., and Li J.-Y. 2016. Ceres: Sulfur deposits and graphitized carbon. *Geophysical Research Letters* 43:1–8.

Hiesinger H., Marchi S., Schmedemann N., Schenk P., Pasckert J. H., Neesemann A., O'Brien D. P., Kneissl T., Ermakov A. I., Fu R. R., Bland M. T., Nathues A., Platz T., Williams D. A., Jaumann R, Castillo-Rogez C., Ruesch O., Schmidt B., Park R. S., and Preusker F. 2016. Cratering on Ceres: Implications for its crust and evolution. *Science* 353:aaf4759.

Licandro J., Campins H., Kelley M., Hargrove K., Pinilla-Alonso N., Cruikshank D., Rivkin A. S., and Emery J. 2011. Cybele: Detection of small silicate grains, water-ice, and organics. *Astronomy & Astrophysics* 525:A34.

Luu J. and Jewitt D. 1996. Color diversity among the Centaurs and Kuiper Belt objects. *Astronomical Journal* 112:2310–2318.

McEwen A. S., Preblich B. S., Turtle E. P., Artemieva N. A., Golombek M. P., Hurst M., Kirk R. L., Burr D. M., and Christensen P. R. 2005. The rayed crater Zunil and interpretations of small impact craters on Mars. *Icarus* 176:351–381.

McKay C. P. and Borucki W. J. 1997. Organic synthesis in experimental impact shocks. *Science* 276:390–392.

McSween H. Y. Jr., Emery J. P., Rivkin A. S., Toplis M. J., Castillo-Rogez J. C., Prettyman T. H., De Sanctis M. C., Pieters C. M., Raymond C. A., and Russell C. T. 2017. Carbonaceous chondrites as analogs for the composition and alteration of Ceres. *Meteoritics & Planetary Science* https://doi.org/10.1111/maps.12947.

Moroz L. V., Arnold G., Korochantsev A. V., and Wasch R. 1998. Natural solid bitumens as possible analogs for cometary and asteroid organics: 1. Reflectance spectroscopy of pure bitumens. *Icarus* 134:253–268.

Nathues A., Hoffmann M., Platz T., Thangjam G. S., Cloutis E. A., Reddy V., Le Corre L., Li J.-Y., Mengel K., Rivkin A., Applin D. M., Schaefer M., Christensen U., Sierks H., Ripken J., Schmidt B. E., Hiesinger H., Sykes M. V., Sizemore H. G., Preusker F., and Russell C. T. 2016. FC colour images of dwarf planet Ceres reveal a complicated geological history. *Planetary and Space Science* 134:122–127.

Oberbeck V. R. 1975. The role of ballistic erosion and sedimentation in lunar stratigraphy. *Reviews of Geophysics and Space Physics* 13:337–362.

Paige D. A., Siegler M. B., Harmon J. K., Neumann G. A., Mazarico E. M., Smith D. E., Zuber M. T., Harju E., Delitsky M. L., and Solomon S. C. 2013. Thermal stability of volatiles in the north polar region of Mercury. *Science* 339:300–303.

Pasckert J. H., Hiesinger H., Ruesch O., Williams D. A., Naß A., Kneissl T., Mest S. C., Buczkowski D. L., Scully J. E. C., Schmedemann N., Jaumann R., Roatsch T., Preusker F., Nathues A., Hoffmann M., Schäfer M., De Sanctis M. C., Raymond C. A., and Russell C. T. 2017. Geologic mapping of the Ac-2 Coniraya Quadrangle of Ceres from NASA's Dawn Mission: Implications for a heterogeneously composed crust. *Icarus*. https://doi.org/10.1016/j.icarus.2017.06.015.

Pendleton Y. J. and Allamandola L. J. 2002. The organic refractory material in the diffuse interstellar medium: Mid-infrared spectroscopic constraints. *The Astrophysical Journal* 138:75–98.

Pieters C. M., Adams J. B., Mouginis-Mark P. J., Zisk S. H., Smith M. O., Head J. W., and McCord T. B. 1985. The nature of crater rays: The Copernicus example. *Journal of Geophysical Research* 90:12,393–12,413.

Pizzarello S., Cooper G. W., and Flynn G. J. 2006. The nature and distribution of the organic material in carbonaceous chondrites and interplanetary dust particles. In *Meteorites and the early solar system II*, edited by Lauretta D. and McSween H. Y. Tucson, Arizona: The University of Arizona Press. pp. 625–651.

Prettyman T. H., Mittlefehldt D. W., Yamashita N., Lawrence D. J., Beck A. W., Feldman W. C., McCoy T. J., McSween H. Y., Toplis M. J., Titus T. N., Tricarico P., Reedy R. C., Hendricks J. S., Forni O., Le Corre L., Li J.-Y., Mizzon H., Reddy V., Raymond C. A., and Russell C. T. 2012. Elemental mapping by Dawn reveals exogenic H in Vesta's regolith. *Science* 338:242–246.

Prettyman T. H., Yamashita N., Toplis M. J., McSween H. Y., Schörghofer N., Marchi S., Feldman W. C., Castillo-

Rogez J., Forni O., Lawrence D. J., Ammannito E., Ehlmann B. L., Sizemore H. G., Joy S. P., Polanskey C. A., Rayman M. D., Raymond C. A., and Russell C. T. 2017. Extensive water ice within Ceres' aqueously altered regolith: Evidence from nuclear spectroscopy. *Science* 355:55–59. https://doi.org/10.1126/science.aah6765.

Raponi A., Carrozzo F. G., Zambon F., De Sanctis M. C., Ciarniello M., Frigeri A., Ammannito E., Tosi F., Combe J.-P., Longobardo A., Palomba E., Pieters C. M., Raymond C. A., and Russell C. T. 2017. Mineralogical mapping of Coniraya Quadrangle of the Dwarf Planet Ceres. *Icarus.* https://doi.org/10.1016/j.icarus.2017.10.023.

Reddy V., Le Correa L., O'Brien D. P., Nathues A., Cloutis E. A., Durda D. D., Bottkee W. F., Bhatt M. U., Nesvorny D., Buczkowski D., Scully J. E. C., Palmer E. M., Sierks H., Mann P. J., Becker K. J., Becki A. W., Mittlefehldt D., Li J.-Y., Gaskell R., Russell C. T., Gaffey M. J., McSween H. Y., McCord T. B., Combe J.-P., and Blewett D. 2012. Delivery of dark material to Vesta via carbonaceous chondritic impacts. *Icarus* 221:544–559.

Rivkin A. S. and Emery J. P. 2010. Detection of ice and organics on an asteroidal surface. *Nature* 464:1322–1323.

Rivkin A. S., Li J. Y., Milliken R. E., Lim L. F., Lovell A. J., Schmidt B. E., McFadden L. A., and Cohen B. A. 2011. The surface composition of Ceres. *Space Science Reviews* 163:95.

Roatsch T., Kersten E., Matz K.-D., Preusker F., Scholten F., Jaumann R., Raymond C. A., and Russell C. T. 2016. High-resolution Ceres High Altitude Mapping Orbit atlas derived from Dawn Framing Camera images. *Planetary and Space Science* 129:103–107.

Russell C. T., Raymond C. A., Ammannito E., Buczkowski D. L., De Sanctis M. C., Hiesinger H., Jaumann R., Konopliv A. S., McSween H. Y., Nathues A., Park R. S., Pieters C. M., Prettyman T. H., McCord T. B., McFadden L. A., Mottola S., Zuber M. T., Joy S. P., Polanskey C., Rayman M. D., Castillo-Rogez J. C., Chi P. J., Combe J. P., Ermakov A., Fu R. R., Hoffmann M., Jia Y. D., King S. D., Lawrence D. J., Li J.-Y., Marchi S., Preusker F., Roatsch T., Ruesch O., Schenk P., Villarreal M. N., and Yamashita N. 2016. Dawn arrives at Ceres: Exploration of a small, volatile-rich world. *Science* 353:1008–1010.

Sandford S. A., Aléon J., Alexander C. M. O'D., Araki T., Bajt S., Baratta G. A., Borg J., Bradley J. P., Brownlee D. E., Brucato J. R., Burchell M. J., Busemann H., Butterworth A., Clemett S. J., Cody G., Colangeli L., Cooper G., D'Hendecourt L., Djouadi Z., Dworkin J. P., Ferrini G., Fleckenstein H., Flynn G. J., Franchi I. A., Fries M., Gilles M. K., Glavin D. P., Gounelle M., Grossemy F., Jacobsen C., Keller L. P., Kilcoyne A. L. D., Leitner J., Matrajt G., Meibom A., Mennella V., Mostefaoui S., Nittler L. R., Palumbo M. E., Papanastassiou D. A., Robert F., Rotundi A., Snead C. J.,

Spencer M. K., Stadermann F. J., Steele A., Stephan T., Tsou P., Tyliszczak T., Westphal A. J., Wirick S., Wopenka B., Yabuta H., Zare R. N., and Zolensky M. E. 2006. Organics captured from Comet 81P/Wild 2 by the Stardust Spacecraft. *Science* 314:1720–1724.

Schmedemann N., Kneissl T., Neesemann A., Stephan K., Jaumann R., Krohn K., Michael G. G., Matz K. D., Otto K. A., Raymond C. A., and Russell C. T. 2016. Timing of optical maturation of recently exposed material on Ceres. *Geophysical Research Letters* 43:11,987–11,993.

Schmedemann N., Neesemann A., Schulzeck F., Krohn K., von der Gathen I., Otto K. A., Jaumann R., Michael G., Raymond C. A., and Russell C. T. 2017. The distribution of impact ejecta on ceres (abstract #1233). 48th Lunar and Planetary Science Conference. CD-ROM.

Schröder S. E., Mottola S., Carsenty U., Ciarniello M., Jaumann R., Li J.-Y., Longobardo A., Palmer E., Pieters C., Preusker F., Raymond C. A., and Russell C. T. 2017. Resolved spectrophotometric properties of the Ceres surface from Dawn Framing Camera images. *Icarus* 288:201–225.

Schultz P. H. and Gault D. E. 1985. Clustered impacts: Experiments and implications. *Journal of Geophysical Research* 90:3701–3732.

Sierks H., Keller H. U., Jaumann R., Michalik H., Behnke T., Bubenhagen F., Büttner I., Carsenty U., Christensen U., Enge R., Fiethe B., Gutiérrez Marqués P., Hartwig H., Krüger H., Kühne W., Maue T., Mottola S., Nathues A., Reiche K.-U., Richards M. L., Roatsch T., Schröder S. E., Szemerey I., and Tschentscher M. 2011. The Dawn framing camera. *Space Science Reviews* 163:263–327.

Soderblom L. A., Barnes J. W., Brown R. H., Clark R. N., Janssen M. A., McCord T. B., Niemann H. B., and Tomasko M. G. 2009. Composition of Titan's surface. In *Titan from Cassini-Huygens*, edited by Brown R. H., Lebreton J.-P. and Waite J. H. New York: Springer. pp. 141–176.

Sykes M. V., Lebofsky L. A., Hunten D. M., and Low F. 1986. The discovery of dust trails in the orbits of periodic comets. *Science* 232:1115–1117.

Takir J. P., Emery H. Y., Mcsween C. A. Jr., Hibbitts R. N., Clark N., and Pearson A. Wang 2013. Nature and degree of aqueous alteration in CM and CI carbonaceous chondrites. *Meteoritics & Planetary Science* 48:1618–1637.

Waite J. H. Jr., Lewis W. S., Magee B. A., Lunine J. I., McKinnon W. B., Glein C. R., Mousis O., Young D. T., Brockwell T., Westlake J., Nguyen M.-J., Teolis B. D., Niemann H. B., McNutt R. L. Jr., Perry M., and Ip W.-H. 2009. Liquid water on Enceladus from observations of ammonia and 40Ar in the plume. *Nature* 460:487–490.

Williams D. A., Buczkowski D. L., Mest S. C., Scully J. E. C., Platz T., and Kneissl T. 2017. Introduction: The geologic mapping of Ceres. *Icarus.* https://doi.org/10.1016/j.icarus.2017.05.004.

SUPPORTING INFORMATION

Additional supporting information may be found in the online version of this article:

Appendix S1. Seven images and image products are provided at high resolution in order to allow evaluation of details for the data and information discussed here.